Single-top transverse-momentum distributions at approximate NNLO

Nikolaos Kidonakis

Department of Physics, Kennesaw State University, Kennesaw, Georgia 30144, USA

(Received 21 October 2015; published 11 March 2016)

I present approximate next-to-next-to-leading-order (aNNLO) transverse-momentum (p_T) distributions in single-top production processes. The aNNLO results are derived from the next-to-next-to-leading-logarithm resummation of soft-gluon corrections in the differential cross section. Single-top as well as single-antitop p_T distributions are shown in t-channel, s-channel, and tW production for LHC energies.

DOI: 10.1103/PhysRevD.93.054022

I. INTRODUCTION

The study of top quarks is a central part of the current collider programs. While the main production mode at the LHC is top-antitop pair production, single-top production is an important set of processes which have been observed at the Tevatron and the LHC.

The production of single tops or single antitops can proceed via three different partonic-channel processes. The numerically dominant one is the t-channel, which involves the exchange of a spacelike W boson, i.e. processes of the form $qb \to q't$ and $\bar{q}b \to \bar{q}'t$ for single-top production, as well as $q\bar{b} \to q'\bar{t}$ and $\bar{q}\,\bar{b} \to \bar{q}'\bar{t}$ for single-antitop production. The numerically smallest single-top process at the LHC is the s-channel, which involves the exchange of a timelike W boson, i.e. processes of the form $q\bar{q}' \to \bar{b}t$ for single-top production and $q\bar{q}' \to b\bar{t}$ for single-antitop production. The third channel is associated tW production, via the processes $bg \to tW^-$ and $\bar{b}g \to \bar{t}W^+$, which is quite significant at the LHC.

The complete next-to-leading-order (NLO) corrections to the differential cross section for t-channel and s-channel production appeared in Ref. [1] and for tW production in Ref. [2]. Further results for the NLO top transverse-momentum, p_T, distributions at LHC energies in t-channel production have appeared in [3–7]; for s-channel production in [8]; and for tW production in [9].

Higher-order corrections (beyond NLO) can be calculated from soft-gluon resummation. Such calculations for single-top production appeared first at next-to-leading-logarithm (NLL) accuracy in Ref. [10]. More recently, calculations were performed at next-to-next-to-leading-logarithm (NNLL) accuracy in the resummation in Ref. [11]. Approximate next-to-next-to-leading-order (aNNLO) corrections were calculated from the NNLL result for t-channel, s-channel, and tW production [11]. As shown and discussed in detail in [10,11], the soft-gluon corrections numerically dominate the cross section, and thus the soft-gluon approximation works very well. The approximate and exact NLO cross sections for single-top production in all channels are within a few percent of each other for all LHC and Tevatron energies, and for the t-channel this is also known to hold at NNLO since the recent results in [12].

The resummation in [10,11] is performed for the double-differential cross section, and thus it enables the calculation of differential distributions in addition to total cross sections. The transverse-momentum distribution of the top or antitop is very interesting because effects due to new physics may appear at large p_T. The calculation of these p_T distributions in all three single-top channels at LHC energies is the topic of this paper. Results for the t-channel p_T distributions have been published before in [13], so here we update them and give new results for the new 13 TeV LHC energy. For the s-channel and tW production we provide new results.

Our work follows the standard moment-space perturbative QCD resummation formalism. Results for t-channel p_T distributions based on another approach, soft-collinear effective theory (SCET), have appeared in [14], and the differences between the moment-space and SCET approaches have been described in [11].

In the next section I describe the kinematics and give some details for the calculation of the aNNLO corrections. We present numerical results for the single-top and single-antitop p_T distributions in the t-channel in Sec. III, in the s-channel in Sec. IV, and in the tW-channel in Sec. V. We conclude in Sec. VI.

II. KINEMATICS FOR aNNLO SINGLE-TOP DISTRIBUTIONS

We study single-top production in collisions of protons A and B with momenta $p_A + p_B \to p_3 + p_4$. The hadronic kinematical variables are $S = (p_A + p_B)^2$, $T = (p_A - p_3)^2$, and $U = (p_B - p_3)^2$. The partonic reactions have momenta $p_1 + p_2 \to p_3 + p_4$. The partonic kinematical variables are $s = (p_1 + p_2)^2$, $t = (p_1 - p_3)^2$, and $u = (p_2 - p_3)^2$, with $p_1 = x_1 p_A$ and $p_2 = x_2 p_B$. We also define the threshold variable $s_4 = s + t + u - m_3^2 - m_4^2$. If we denote the top-quark mass by m_t and the W-boson mass by m_W, then for t-channel and s-channel production $m_3 = 0$ and $m_4 = m_t$, while for tW production $m_3 = m_t$ and $m_4 = m_W$. We note that s_4 vanishes at partonic threshold for each process.

The resummation of soft-gluon corrections follows from the factorization of the differential cross section into hard, soft, and jet functions in the partonic processes [10,11]. The resummed result is then used to generate approximate higher-order corrections. The soft-gluon corrections have the form of logarithmic plus distributions, $[\ln^k(s_4/m_t^2)/s_4]_+$, where $0 \le k \le 2n-1$ for the nth order perturbative QCD corrections. The approximate NNLO soft-gluon corrections to the double-differential partonic cross section, $d^2\hat{\sigma}/(dtdu)$, are of the form

$$\frac{d^2\hat{\sigma}^{(2)}}{dtdu} = F_{\rm LO}\frac{\alpha_s^2}{\pi^2}\sum_{k=0}^{3} C_k^{(2)}\left[\frac{\ln^k(s_4/m_t^2)}{s_4}\right]_+, \qquad (1)$$

where α_s is the strong coupling, and $F_{\rm LO}$ denotes the leading-order (LO) contributions, i.e. $d^2\hat{\sigma}^{(0)}/(dtdu) = F_{\rm LO}\delta(s_4)$. The aNNLO coefficients $C_k^{(2)}$ are in general different for each partonic process. The leading coefficient, $C_3^{(2)}$, depends only on color factors and it equals $3C_F$ for t-channel and s-channel production, and $2(C_F+C_A)$ for tW production, where $C_F = (N_c^2-1)/(2N_c)$ and $C_A = N_c$, with $N_c = 3$ being the number of colors. The subleading coefficients $C_2^{(2)}$, $C_1^{(2)}$, and $C_0^{(2)}$ are in general functions of s, t, u, m_t, and the factorization scale μ_F, and (for $C_1^{(2)}$ and $C_0^{(2)}$) also the renormalization scale μ_R. These coefficients have been determined from two-loop calculations for all partonic processes contributing to these channels [10,11]. NLL resummation [10] is sufficient to calculate all aNNLO coefficients except $C_0^{(2)}$, which is fully determined only by NNLL resummation [11]. The one-loop soft-anomalous dimension [10,11] for each process contributes to all subleading coefficients, while the two-loop soft-anomalous dimension [11] for each process contributes to $C_0^{(2)}$.

For the t-channel processes $qb \to q't$ the LO terms are

$$F_{\rm LO}^{qb\to q't} = \frac{\pi\alpha^2 V_{tb}^2 V_{qq'}^2}{\sin^4\theta_W}\frac{(s-m_t^2)}{4s(t-m_W^2)^2}. \qquad (2)$$

Here $\alpha = e^2/(4\pi)$, V_{ij} are elements of the Cabibbo-Kobayashi-Maskawa matrix, and θ_W is the weak mixing angle.

For the t-channel processes $\bar{q}b \to \bar{q}'t$ the LO terms are

$$F_{\rm LO}^{\bar{q}b\to \bar{q}'t} = \frac{\pi\alpha^2 V_{tb}^2 V_{qq'}^2}{\sin^4\theta_W}\frac{[(s+t)^2-(s+t)m_t^2]}{4s^2(t-m_W^2)^2}. \qquad (3)$$

For the s-channel processes $q\bar{q}' \to \bar{b}t$ the LO terms are

$$F_{\rm LO}^{q\bar{q}'\to \bar{b}t} = \frac{\pi\alpha^2 V_{tb}^2 V_{qq'}^2}{\sin^4\theta_W}\frac{t(t-m_t^2)}{4s^2(s-m_W^2)^2}. \qquad (4)$$

For the associated production process $bg \to tW^-$ the LO terms are

$$F_{\rm LO}^{bg\to tW^-} = \frac{\pi V_{tb}^2\alpha_s\alpha}{12m_W^2\sin^2\theta_W s^2}\left(\frac{A_1}{(u-m_t^2)^2} - \frac{2A_2}{(u-m_t^2)s} + \frac{2A_3}{s^2}\right), \qquad (5)$$

where $A_1 = -(u-m_W^2)(s-m_t^2-m_W^2)(2m_W^2+m_t^2)/2 - (t-m_t^2)(-2m_W^4+m_W^2m_t^2+m_t^4)/2 - 2(u-m_W^2)m_t^2(2m_W^2+m_t^2)$; $A_2 = -(t-m_t^2)(-m_W^2+m_t^2)m_W^2 - (u-m_W^2)\times(t-m_t^2)m_t^2/2 - (u-m_t^2)(u-m_W^2)m_t^2/2 - sm_W^2m_t^2 - sm_t^4/2$; and $A_3 = -s(u-m_t^2)(2m_W^2+m_t^2)/4$.

To calculate the hadronic differential cross section we convolute the partonic cross section with parton distribution functions (pdf's). We use the MSTW2008 NNLO pdf [15] in our numerical results below unless otherwise noted. We do that for consistency with the results shown in our previous work [11]. But we also discuss results using the recent MMHT 2014 NNLO pdf [16]. As we will see, the shape of the distributions is not affected by this choice of pdf for any of our results.

The transverse-momentum distribution of the top quark (or of the antitop) is given by

$$\frac{d\sigma}{dp_T} = 2p_T\int_{Y^-}^{Y^+} dY\int_{x_2^-}^{1} dx_2\int_0^{s_{4\,\rm max}} ds_4\frac{x_1x_2S}{x_2S+T_1} \times\phi(x_1)\phi(x_2)\frac{d^2\hat{\sigma}}{dtdu}, \qquad (6)$$

where ϕ denotes the pdf; Y is the top-quark rapidity, $Y^\pm = \pm(1/2)\ln[(1+\beta_T)/(1-\beta_T)]$, with $\beta_T = [1-4(m_3^2+p_T^2)S/(S+m_3^2-m_4^2)^2]^{1/2}$; $x_1 = (s_4-m_3^2+m_4^2-x_2U_1)/(x_2S+T_1)$, with $T_1 = T-m_3^2 = -\sqrt{S}(m_3^2+p_T^2)^{1/2}e^{-Y}$ and $U_1 = U-m_3^2 = -\sqrt{S}(m_3^2+p_T^2)^{1/2}e^{Y}$; $x_2^- = (m_4^2-T)/(S+U_1)$; and $s_{4\,\rm max} = x_2(S+U_1)+T-m_4^2$. In particular, using Eq. (1) and the properties of plus distributions, the aNNLO corrections to the p_T distribution can be written as

$$\frac{d\sigma^{(2)}}{dp_T} = \frac{\alpha_s^2}{\pi^2}2p_T\int_{Y^-}^{Y^+} dY\int_{x_2^-}^{1} dx_2\phi(x_2)\left\{\int_0^{s_{4\rm max}} ds_4\sum_{k=0}^{3}\frac{1}{s_4}\ln^k\left(\frac{s_4}{m_t^2}\right)\right. \times\left[F_{\rm LO}C_k^{(2)}\frac{x_1x_2S}{x_2S+T_1}\phi(x_1) - F_{\rm LO}^{\rm el}C_k^{(2)\,\rm el}\frac{x_1^{\rm el}x_2S}{x_2S+T_1}\phi(x_1^{\rm el})\right] \left. + \sum_{k=0}^{3}\frac{1}{k+1}\ln^{k+1}\left(\frac{s_{4\rm max}}{m_t^2}\right)F_{\rm LO}^{\rm el}C_k^{(2)\,\rm el}\frac{x_1^{\rm el}x_2S}{x_2S+T_1}\phi(x_1^{\rm el})\right\}. \qquad (7)$$

Here the elastic versions of x_1, $F_{\rm LO}$, and $C_k^{(2)}$, denoted by the superscript "el," refer to these variables calculated with the constraint $s_4 = 0$. We note that the total cross section can be obtained by integrating the p_T distribution from 0 to $p_{T\,\mathrm{max}} = [(S - m_3^2 - m_4^2)^2 - 4m_3^2 m_4^2]^{1/2}/(2\sqrt{S})$, and we have checked for consistency that we find the total cross section results of [11], which are also in excellent agreement with LHC and Tevatron data in all three channels (see Ref. [17] for comparisons with recent data).

III. t-CHANNEL p_T DISTRIBUTIONS

We begin with t-channel single-top production. The total cross section at 13 TeV energy at the LHC for a top-quark mass $m_t = 173.3$ GeV is $136^{+3}_{-1} \pm 3$ pb for single-top production and $82^{+2}_{-1} \pm 2$ pb for single-antitop production in the t-channel using the MSTW 2008 NNLO pdf [15]. The central results are with $\mu_F = \mu_R = m_t$. The theoretical uncertainty of the cross section consists of two parts: the first one is from scale variation by a factor of 2 (i.e. from $m_t/2$ to $2m_t$), and the second one is from the MSTW pdf [15] uncertainties at 90% C.L. It is seen that the pdf uncertainties are somewhat larger than the scale uncertainties.

We note that the difference is very small if instead we use the MMHT 2014 NNLO pdf [16]; in that case we find $138^{+3}_{-1} \pm 2$ pb for single-top production and $83^{+2}_{-1} \pm 1$ pb for single-antitop production, where the first uncertainty is from scale variation and the second uncertainty is from the MMHT pdf at 68% C.L. We observe that although the central values and scale uncertainties are very close whether one uses the MSTW or MMHT pdf, the pdf uncertainties in the two cases are quite different because they are 90% C.L. (i.e. more conservative) for the former and 68% C.L. for the latter. In the figures below we use the MSTW 2008 pdf unless otherwise indicated.

In Fig. 1 we present at 7, 8, 13, and 14 TeV LHC energy the central aNNLO results in the t-channel for the top-quark p_T distribution in the left plot as well as for the antitop p_T distribution in the right plot. The p_T range displayed is up to 500 GeV and the vertical logarithmic scales in the two plots are chosen to be the same for ease of comparison of the relative magnitude of the distributions.

In Fig. 2 we present linear plots for the aNNLO p_T distribution for the top (left panel) and the antitop (right panel) in t-channel production at 13 TeV LHC energy. We also show the theoretical uncertainty by providing upper and lower values (the dashed lines). As we noted for the total cross section, the majority of the uncertainty is due to the pdf. The top p_T distributions peak at a p_T of around 36 GeV, and the aNNLO corrections provide a small enhancement of 1% over the NLO result calculated with the same pdf. The inset plot shows the ratio of the aNNLO and NLO distributions at high p_T values. The enhancement diminishes at large p_T; we note, however, that we do not perform a targeted large-p_T resummation.

We note that the shape of the distributions is unaffected (to the per mill level) if the MMHT 2014 pdf is instead used. There is only a very small overall normalization change, as for the cross section. If one plots the normalized distribution $(1/\sigma)d\sigma/dp_T$ using the two different pdf's, then the two curves are indistinguishable. In Fig. 3 we plot the t-channel top (left panel) and antitop (right panel) normalized p_T distributions at 7, 8, 13, and 14 TeV LHC energies.

IV. s-CHANNEL p_T DISTRIBUTIONS

We continue with s-channel single-top production. The total cross section at 13 TeV energy at the LHC for a top-quark mass $m_t = 173.3$ GeV is $7.07 \pm 0.13^{+0.24}_{-0.22}$ pb for single-top production and $4.10 \pm 0.05^{+0.14}_{-0.16}$ pb for single-antitop production in the s-channel. As before, the theoretical uncertainty consists of two parts: the first one is from scale variation by a factor of 2, and the second and larger one is from the MSTW pdf [15] 90% C.L. uncertainties. Again, we note that the difference is very small if instead we use the MMHT 2014 NNLO pdf [16]; in that case we

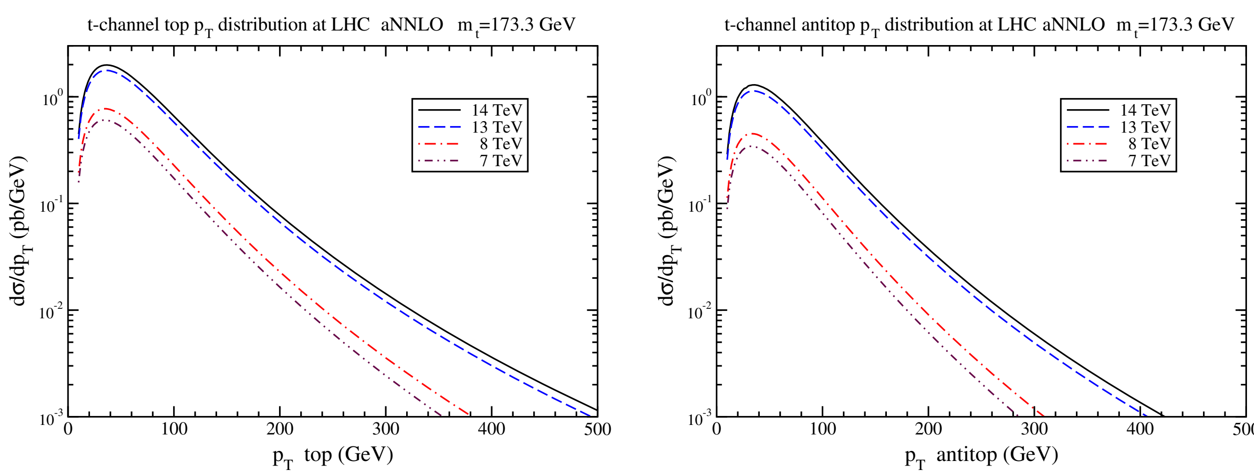

FIG. 1. Approximate NNLO top (left panel) and antitop (right panel) t-channel p_T distributions at 7, 8, 13, and 14 TeV LHC energy.

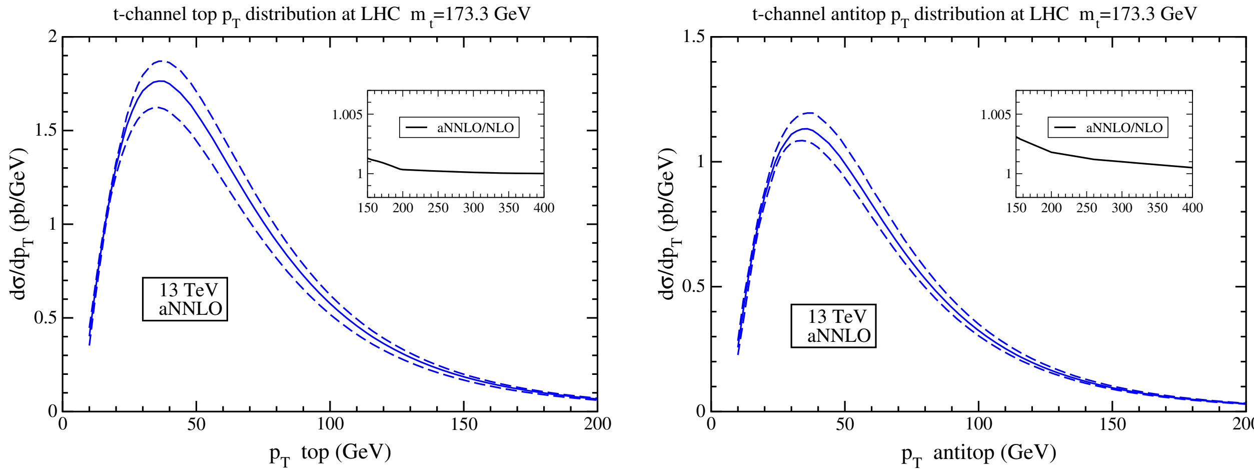

FIG. 2. Approximate NNLO top (left panel) and antitop (right panel) t-channel p_T distributions at 13 TeV LHC energy, with theoretical uncertainty displayed by the dashed lines.

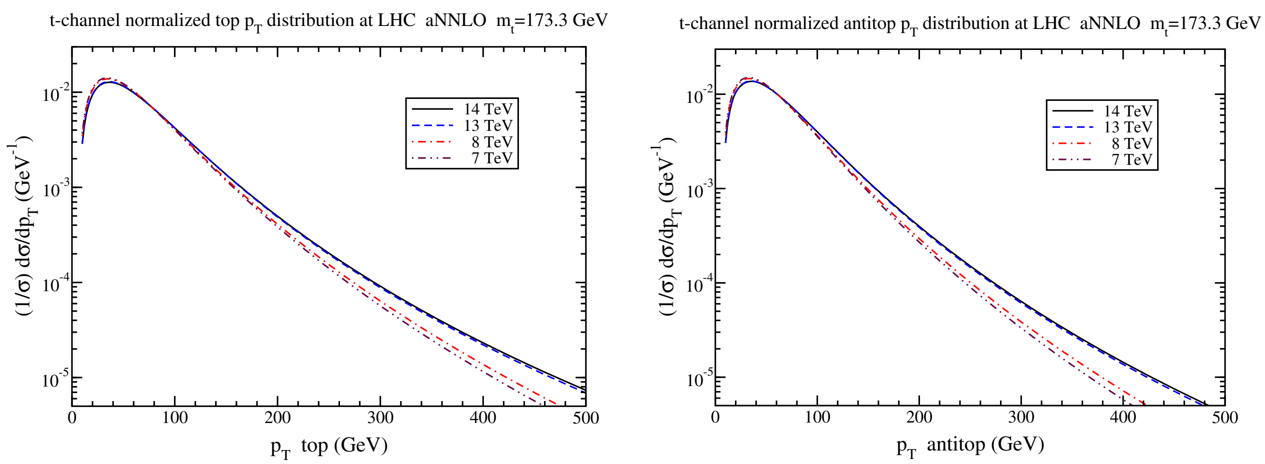

FIG. 3. Approximate NNLO top (left panel) and antitop (right panel) t-channel normalized p_T distributions at 7, 8, 13, and 14 TeV LHC energy.

find $7.15 \pm 0.13^{+0.15}_{-0.17}$ pb for single-top production and $4.14 \pm 0.05 \pm 0.10$ pb for single-antitop production, where the pdf uncertainty is at 68% C.L.

In the s-channel, the enhancement from the NNLO soft-gluon corrections is significant, in contrast to the t-channel. We find an enhancement of over 8% for the total aNNLO s-channel cross section relative to NLO.

In Fig. 4 we present the s-channel central aNNLO results for the top-quark p_T distribution in the left plot as well as for the antitop p_T distribution in the right plot at 7, 8, 13, and 14 TeV LHC energy. The p_T range displayed is up to 320 GeV and the vertical logarithmic scales in the two plots are again chosen to be identical.

In Fig. 5 we present linear plots for the aNNLO p_T distribution for the top (left panel) and the antitop (right panel) in s-channel production at 13 TeV LHC energy. As before, we show the theoretical uncertainty by providing upper and lower values. The top p_T distributions peak at a p_T of around 28 GeV, and the aNNLO corrections provide a large enhancement over the NLO result. The inset plot shows the ratio aNNLO/NLO at high p_T, where the enhancement is smaller.

Again, we note that the shape of the distributions is unaffected if the MMHT 2014 pdf is instead used. In Fig. 6 we plot the s-channel top (left panel) and antitop (right panel) normalized p_T distributions, $(1/\sigma)d\sigma/dp_T$, at 7, 8, 13, and 14 TeV LHC energies.

V. tW-CHANNEL p_T DISTRIBUTIONS

Finally, we discuss tW production. The total cross section at 13 TeV energy at the LHC for a top-quark mass $m_t = 173.3$ GeV using the MSTW 2008 pdf [15] is $35.2 \pm 0.9^{+1.6}_{-1.7}$ pb for tW^- production, and it is the same for $\bar{t}W^+$ production. Again, the theoretical uncertainty comes from scale variation by a factor of 2, and from the 90% C.L. pdf uncertainty; the latter is almost a factor of 2 larger. Again, we note that the difference is very small if instead we use

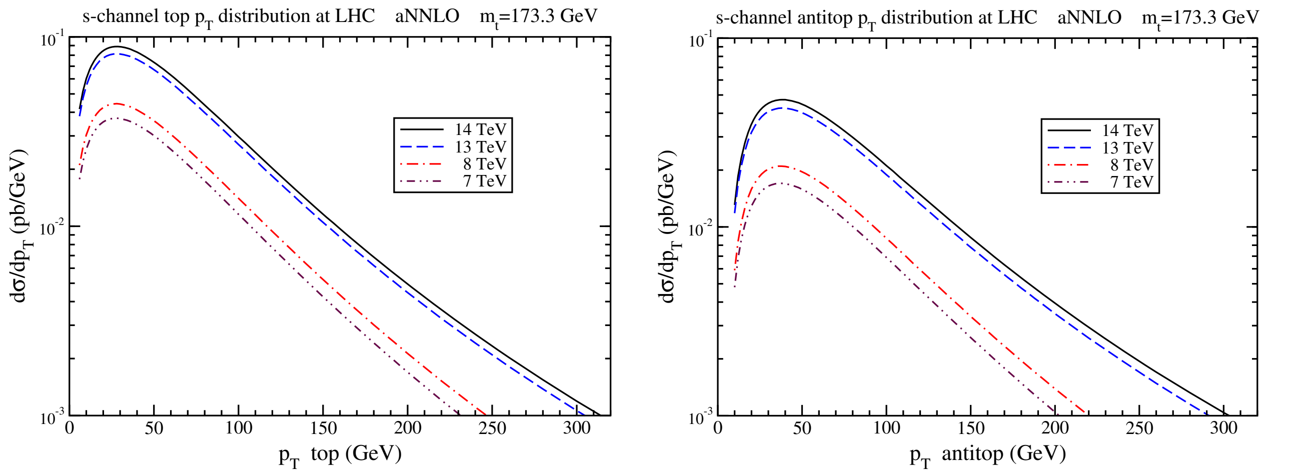

FIG. 4. Approximate NNLO top (left panel) and antitop (right panel) s-channel p_T distributions at 7, 8, 13, and 14 TeV LHC energy.

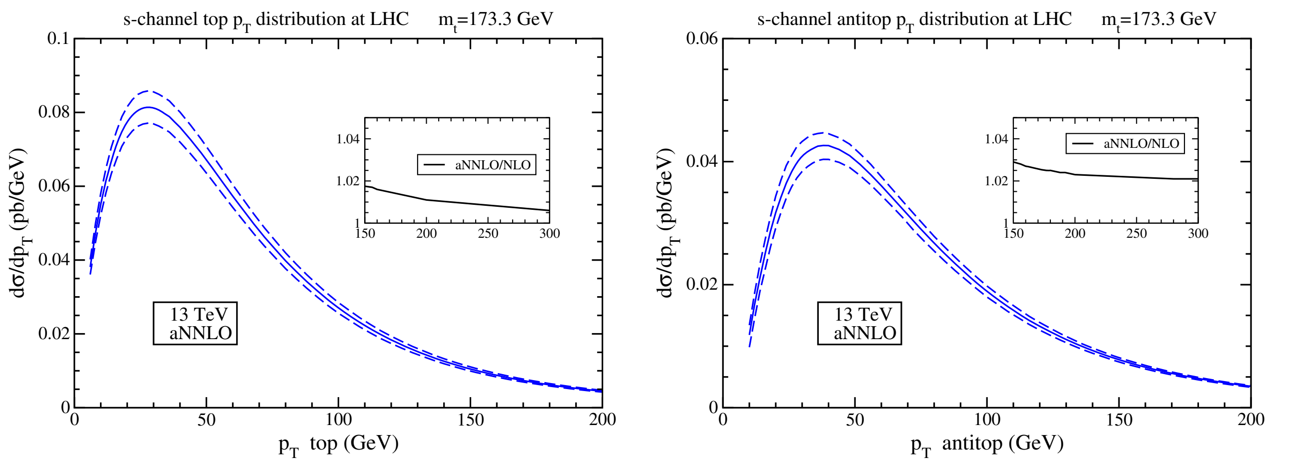

FIG. 5. Approximate NNLO top (left panel) and antitop (right panel) s-channel p_T distributions at 13 TeV LHC energy, with theoretical uncertainty displayed by the dashed lines.

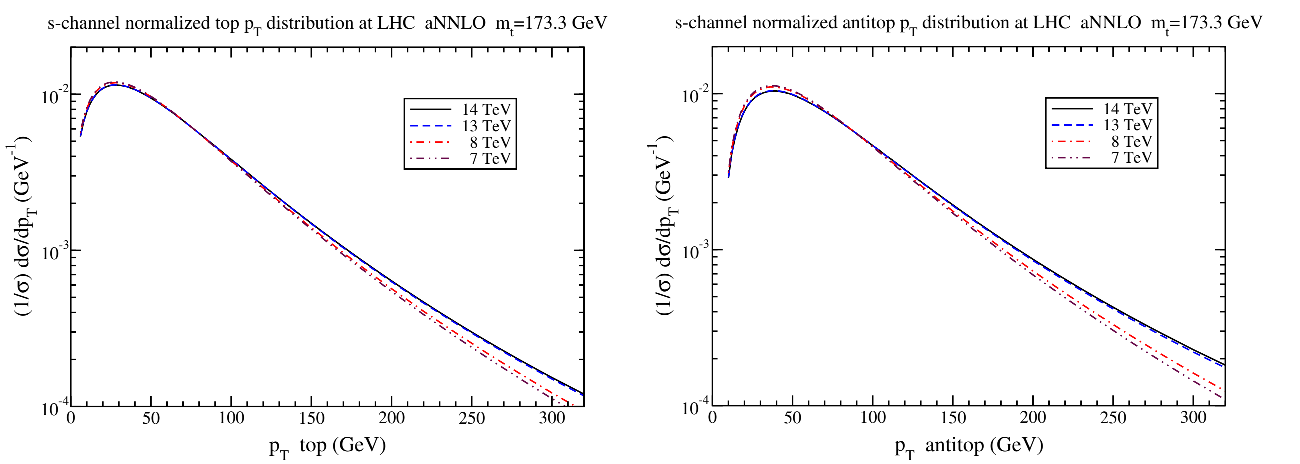

FIG. 6. Approximate NNLO top (left panel) and antitop (right panel) normalized s-channel p_T distributions at 7, 8, 13, and 14 TeV LHC energy.

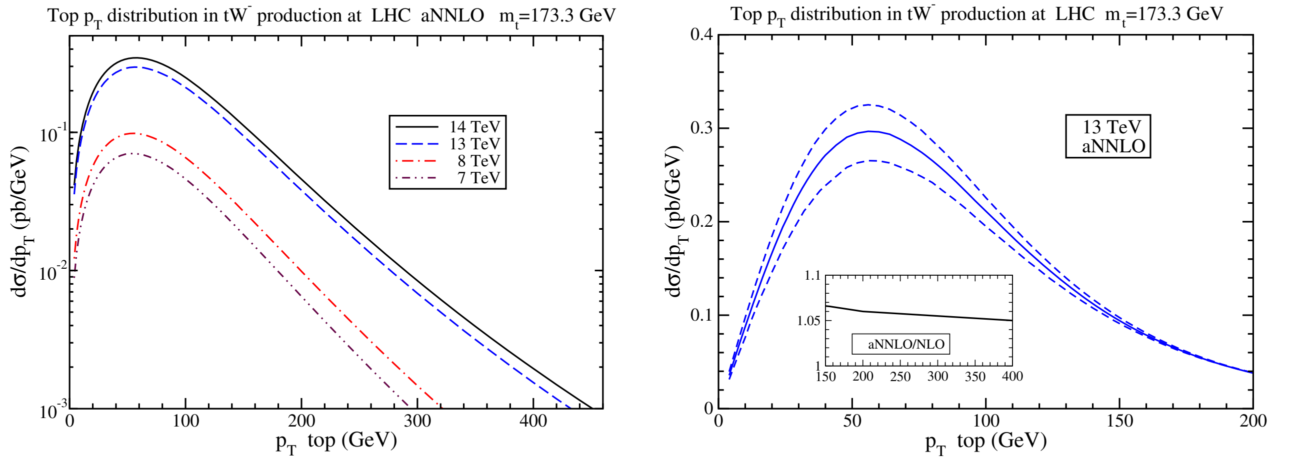

FIG. 7. Approximate NNLO top-quark p_T distributions in the tW channel at (left panel) 7, 8, 13, and 14 TeV LHC energy, and (right panel) at 13 TeV, with the theoretical uncertainty displayed.

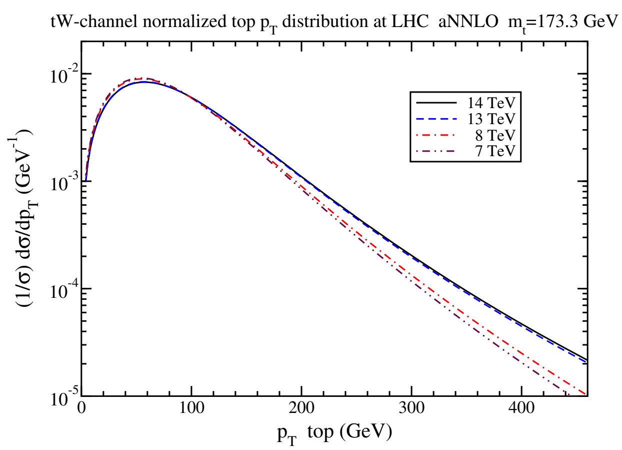

FIG. 8. Approximate NNLO tW-channel normalized top p_T distributions at 7, 8, 13, and 14 TeV LHC energy.

the MMHT 2014 NNLO pdf [16]; in that case we find $36.3 \pm 0.9 \pm 0.9$ pb, where again the pdf uncertainty is at 68% C.L.

The enhancement from the NNLO soft-gluon corrections is also large in the tW-channel. We find an 8% increase for the total aNNLO tW cross section relative to NLO.

In the left plot of Fig. 7 we present the central aNNLO results for the top-quark p_T distribution in tW^- production at 7, 8, 13, and 14 TeV LHC energy. In the right plot of Fig. 7 we present a linear plot for the aNNLO top p_T distribution in tW^- production at 13 TeV LHC energy. We also show the theoretical uncertainty by providing upper and lower values. The top p_T distributions peak at a p_T of around 56 GeV, and the aNNLO corrections provide a substantial enhancement of 8.5% over the NLO result. The inset plot shows the ratio aNNLO/NLO at high p_T. The p_T distributions for the antitop in this channel are the same as for the top.

Once again, we note that the shape of the distributions is unaffected if the MMHT 2014 pdf is instead used. In Fig. 8 we plot the tW-channel normalized top p_T distributions, $(1/\sigma)d\sigma/dp_T$, at 7, 8, 13, and 14 TeV LHC energies.

VI. CONCLUSIONS

I have presented the single-top and single-antitop transverse-momentum distributions at approximate NNLO by including soft-gluon corrections derived from NNLL resummation. Results were presented at 7, 8, 13, and 14 LHC energies for t-channel, s-channel, and tW production. We have paid particular attention to the current 13 TeV LHC energy and have also provided theoretical uncertainties. The corrections are large and very significant in s-channel and tW production but they are rather small in t-channel production.

ACKNOWLEDGMENTS

This material is based upon work supported by the National Science Foundation under Grant No. PHY 1519606.

[1] B. W. Harris, E. Laenen, L. Phaf, Z. Sullivan, and S. Weinzierl, Phys. Rev. D **66**, 054024 (2002).
[2] S.-h. Zhu, Phys. Lett. B **524**, 283 (2002); **537**, 351(E) (2002).
[3] J. M. Campbell, R. Frederix, F. Maltoni, and F. Tramontano, Phys. Rev. Lett. **102**, 182003 (2009).
[4] R. Schwienhorst, C.-P. Yuan, C. Mueller, and Q.-H. Cao, Phys. Rev. D **83**, 034019 (2011).
[5] P. Falgari, F. Giannuzzi, P. Mellor, and A. Signer, Phys. Rev. D **83**, 094013 (2011).
[6] R. Frederix, E. Re, and P. Torrielli, J. High Energy Phys. 09 (2012) 130.
[7] P. Falgari, J. Phys. Conf. Ser. **452**, 012016 (2013).
[8] S. Heim, Q.-H. Cao, R. Schwienhorst, and C.-P. Yuan, Phys. Rev. D **81**, 034005 (2010).
[9] E. Re, Eur. Phys. J. C **71**, 1547 (2011).
[10] N. Kidonakis, Phys. Rev. D **74**, 114012 (2006); **75**, 071501 (R) (2007).
[11] N. Kidonakis, Phys. Rev. D **83**, 091503(R) (2011); **81**, 054028 (2010); **82**, 054018 (2010); Phys. Part. Nucl. **45**, 714 (2014).
[12] M. Brucherseifer, F. Caola, and K. Melnikov, Phys. Lett. B **736**, 58 (2014).
[13] N. Kidonakis, Phys. Rev. D **88**, 031504(R) (2013).
[14] J. Wang, C. S. Li, and H. X. Zhu, Phys. Rev. D **87**, 034030 (2013).
[15] A. D. Martin, W. J. Stirling, R. S. Thorne, and G. Watt, Eur. Phys. J. C **63**, 189 (2009).
[16] L. A. Harland-Lang, A. D. Martin, P. Molytinski, and R. S. Thorne, Eur. Phys. J. C **75**, 204 (2015).
[17] N. Kidonakis, *Proc. Sci.*, DIS2015 (2015) 170 [arXiv: 1506.04072]; in *Proceedings of the Division of Particles and Fields 2015 (DPF 2015), Ann Arbor, MI, 2015*, edited by M. Tecchio and D. Levin (SLAC Report No. C150804, 2015).